

## A composite crack model for concrete based on meshless method

Xin-zheng Lu<sup>†</sup>, Jian-jing Jiang<sup>‡</sup> and Lie-ping Ye<sup>‡†</sup>

Department of Civil Engineering, Tsinghua University, Beijing 100084, China

(Received August 11, 2004, Revised November 17, 2005, Accepted February 3, 2006)

**Abstract.** A crack model for the fracture in concrete based on meshless method is proposed in this paper. The cracks in concrete are classified into micro-cracks or macro-cracks respectively according to their widths, and different numerical approaches are adopted for them. The micro-cracks are represented with smeared crack approach whilst the macro-cracks are represented with discrete cracks that are made up with additional nodes and boundaries. The widely used meshless method, Element-free Galerkin method, is adopted instead of finite element method to model the concrete, so that the discrete crack approach is easier to be implemented with the convenience of arranging node distribution in the meshless method. Rotating-Crack-Model is proved to be preferred over Fixed-Crack-Model for the smeared cracks of this composite crack model due to its better performance on mesh bias. Numerical examples show that this composite crack model can take advantage of the positive characteristics in the smeared and discrete approaches, and overcome some of their disadvantages.

**Keywords:** composite crack; meshless; concrete crack; smeared crack; discrete crack.

---

### 1. Introduction

Concrete is a typical low tensile strength material. Therefore most concrete structures have cracks. The simulation of cracking is a key problem for the numerical analysis of concrete, as well as a most difficult one. Generally there are three methods to simulate the cracks in concrete (Rots and Blaauwendraad 1989, Jiang *et al.* 2005, Bazant and Planas 1997), which are referred as discrete crack methods, smeared crack methods and embedded crack methods, respectively.

The discrete crack method or discrete crack approach (Rots and Blaauwendraad 1989, Jiang *et al.* 2005) represents the cracks with the boundaries of elements and continuously remeshes the elements with the crack propagation. This method can clearly present the propagation path and width of individual cracks. And by adding interfacial elements, it can simulate the aggregation interlock on the crack surface. However, for concrete structures with normal reinforcement, a lot of efforts are needed for discrete crack approaches to simulate a large number of micro-cracks or macro-cracks in concrete.

The smeared crack method or smeared crack approach (Rots and Blaauwendraad 1989, Jiang *et al.* 2005) is used most widely in common finite element (FE) codes. The cracks in concrete are

---

<sup>†</sup> Ph.D., Lecturer, Corresponding author, E-mail: luxinzheng@263.net

<sup>‡</sup> Ph.D., Professor, E-mail: jiang-jj@mail.tsinghua.edu.cn

<sup>‡†</sup> Ph.D., Professor, E-mail: ylp@mail.tsinghua.edu.cn

represented with a zero or negative tension stiffness in the material constitutive law. This method can simulate the large quantities of cracks in concrete, and it is easy to embedded into common FE codes, because cracking is modeled as a material behavior so it does not need to remesh FE model due to cracking. But it is difficult for this method to obtain the information such as the width or propagation path of a certain crack.

The embedded crack model creates special elements with embedded discontinuities to represent the cracks inside the element (Grootenboer *et al.* 1981, Jirasek and Zimmerman 1998, Wells and Sluys 2000, Zi and Belytschko 2003, Areias and Belytschko 2005, Gasser and Holzapfel 2005, Areias and Belytschko 2005, Loblein and Schroder 2005, Schroder and Loblein 2005). It is also a convenient method to avoid remeshing. This method initiated more than 20 years ago (Grootenboer *et al.* 1981) and recent years it has received more focus. Some new conceptions with embedded discontinuities such as Partition of Unity Finite Element Method (PUFEM) (Gasser and Holzapfel 2005) or extend Finite Element Method (XFEM) (Zi and Belytschko 2003, Areias and Belytschko 2005), are developed and introduced in concrete cracking simulation to overcome the drawbacks of discrete or smeared crack models.

After all, discrete and smeared crack models are still the most popular methods in concrete fracture simulations. And for the extremely large number of micro-cracks in concrete, the smeared crack approach is believed to be the most effective method to represent them. And some important researches have been carried out to combine the smeared and discrete approaches to take their advantages and to avoid their drawbacks (Munjiza *et al.* 1999, Munjiza 2004). But with finite element method large efforts are still needed for remeshing of the discrete cracks. So the meshless method, in which no element mesh is needed, can be introduced to replace finite element method for discrete crack simulation, whilst micro-cracks of concrete are still simulated with smeared crack approach.

## 2. Element-free Galerkin method

### 2.1 Basic theory of element-free Galerkin method

The meshless method has many different branches (Liu 2002). And the meshless method used in this paper is the widely used element-free Galerkin method (EFGM), which was developed by Belytschko (Belytschko and Lu 1994, Belytschko 1996). Its basic procedure is expressed as follows:

For a field function  $u^*(x)$  in a domain of  $\Omega$ , its approximate function can be built as:

$$u^*(x) \approx u^h(x) = \sum_{j=1}^m p_j(x) a_j(x) \equiv \mathbf{p}^T(x) \mathbf{a}(x) \quad (1)$$

where  $\mathbf{a}(x)$  is the factor vector, which is a function of  $x$ , and  $\mathbf{p}(x)$  is an  $m$ -dimensional polynomial. In this study, a linear polynomial  $\mathbf{p}(x)$  is adopted so that for planar problems:

$$\mathbf{p}^T(x) = [1 \ x \ y] \quad (m = 3) \quad (2)$$

The approximation of Eq. (1) around point  $x^*$  is

$$u^h(x, x^*) = \sum_{j=1}^m p_j(x^*) a_j(x) \equiv \mathbf{p}^T(x^*) \mathbf{a}(x) \quad (3)$$

Factor  $\mathbf{a}(x)$  will be determined by weighted moving least-square (MLS) fitting for the local approximation, which is obtained by minimizing the difference between the local approximation and the original function. This yields the following quadratic form:

$$J = \sum_{j=1}^n w(\|x - x_j\|) [u^h(x, x_j) - u^*(x_j)]^2 = \sum_{j=1}^n w(\|x - x_j\|) \left[ \sum_{i=1}^m p_i(x_j) a_i(x) - u^*(x_j) \right]^2 \quad (4)$$

where  $w(\|x - x_j\|)$  is the weight function, and  $u^*(x_j)$  is the value of  $u^*(x)$  on point  $x_j$ .

Minimizing  $J$  to the factor  $\mathbf{a}(x)$ , that is,  $\partial J / \partial a_i = 0$ . Then yielding the factor  $\mathbf{a}(x)$

$$\mathbf{a}(x) = A^{-1}(x)B(x)\mathbf{u}^* \quad (5)$$

where

$$A(x) = \sum_{i=1}^n w_i(\|x - x_i\|) p(x_i) p^T(x_i) \quad (6a)$$

$$B(x) = [w_1(\|x - x_1\|)p(x_1), \dots, w_n(\|x - x_n\|)p(x_n)] \quad (6b)$$

$$\mathbf{u}^* = [u^*(x_1), u^*(x_2), \dots, u^*(x_n)]^T \quad (6c)$$

So, Eq. (1) can be re-written as

$$u^h(x) = \sum_{i=1}^n n_i(x) u_i^* \quad (7)$$

where

$$n_i(x) = \sum_{j=1}^m p_j(x) [A^{-1}(x)B(x)]_{ji} \quad (8)$$

The partial difference of function  $n_i(x)$  is

$$n_{i,k}(x) = \sum_{j=1}^m \{ p_{j,k}(x) [A^{-1}(x)B(x)]_{ji} + p_j(x) [A_{,k}^{-1}(x)B(x) + A^{-1}(x)B_{,k}(x)]_{ji} \} \quad (9)$$

where

$$A_{,k}^{-1}(x) = -A^{-1} A_{,k} A^{-1} \quad (10)$$

And the global stiffness matrix will be obtained by

$$K = \int_{\Omega} B^T D B d\Omega \quad (11)$$

where for planar problems,

$$B = \begin{bmatrix} n_{1,x} & 0 & n_{2,x} & 0 & \dots & n_{n,x} & 0 \\ 0 & n_{1,y} & 0 & n_{2,y} & \dots & 0 & n_{n,y} \\ n_{1,y} & n_{1,x} & n_{2,y} & n_{2,x} & \dots & n_{n,y} & n_{n,x} \end{bmatrix} \quad (12)$$

## 2.2 Parameters in EFGM implementation

The weight function which is developed by Zhou and Kou (1998) is chosen in this study:

$$w(r_i) = \frac{r_{mi}^2}{r_i^2 + \varepsilon^2 r_{mi}^2} \left[ 1 - \frac{r_i^2}{r_{mi}^2} \right]^k \quad (13)$$

where  $\varepsilon=0.05$ ,  $k=2$ .  $r_m$  is the radius of influence domain. It will be set automatically by the program, parallel with the changing of node distribution and boundary distribution. The boundary conditions are applied with the penalty function method, which means the displacement boundary condition is applied with a large penalty multiplier (Luis Gavete and Benito 2000).

## 3. Influence domain size with discrete cracks

With the propagation of discrete cracks, the relationships between the nodes and Gauss integration points change continuously. The following method is adopted to set up the size of the influence domain in EFGM, and to build up the relationships between nodes and Gauss integration points.

- (1) For a certain Gauss integration point  $P_{int}$ , it is linked with every node with straight lines. If a line between  $P_{int}$  and a node intersects some boundaries, which may be the edge of the specimen or the surface of a crack, then the corresponding nodes will be considered as being “shadowed” by the boundaries. And this node will not attend the following computation of this Gauss point.
- (2) For all nodes which are not “shadowed”, the closest 6 nodes are selected to attend the moving least square (MLS) computation to buildup the approximate displacement field.
- (3) And the distance from  $P_{int}$  to the farthest one of the 6 nodes that attends the MLS computation is set as the influence domain radius  $r_m$  in Eq. (13).

An example for the relationship between nodes and Gauss integration points obtained by the above procedure is shown in Fig. 1. These steps are repeated for every Gauss point so that all the geometrical parameters needed in EFGM will be obtained.

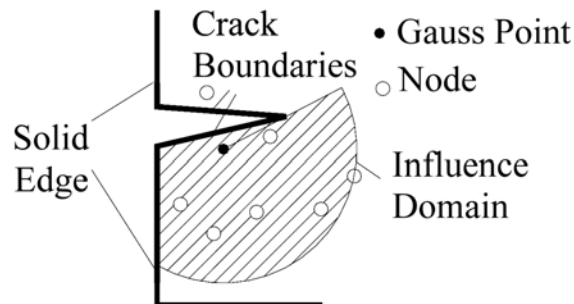


Fig. 1 Influence domain and its border

## 4. Initiation and propagation of macro-cracks

### 4.1 Classification for the cracks

The tensile strain corresponding to concrete tensile strength is very small, which is only about  $10^{-4}$ . So in the real concrete structures with normal reinforcement, there are many invisible micro-cracks. It is almost impossible to simulate these micro-cracks one by one by discrete crack methods. And at the same time, the widths or the shapes of cracks that are mostly concerned in practice are those visible macro-cracks. Hence, it is rational to treat different cracks with different models, which is shown as follows:

- (1) If the tensile strain of concrete is less than a certain value  $\varepsilon_{i,u}$ , the cracks corresponding to this strain are considered as micro-cracks. For these cracks, smeared crack approach is adopted because it is easier to represent the average behavior of a number of micro-cracks.
- (2) When the tensile strain of concrete is larger than  $\varepsilon_{i,u}$ , it is supposed that there are some macro-cracks in the concrete. And the smeared crack model cannot describe these cracks precisely. Hence, new nodes and boundaries are added into the numerical model to describe the discrete macro-cracks.

From the above description it can be found that the criterion between micro and macro-cracks is based on the tensile strain  $\varepsilon_{i,u}$  of concrete. In this study, a tension strain when the residual tension stress of cracked concrete decreases to zero is adopted for  $\varepsilon_{i,u}$ . There are two reasons for choosing such value of  $\varepsilon_{i,u}$ . The first reason is that when tension strain is larger than  $\varepsilon_{i,u}$ , there is no residual tension stress in cracked concrete, so no more interfacial elements are needed for discrete cracks to describe the residual tension stress, which will simplify the implementation of discrete cracks. The second reason is that as no residual tension stress in cracked concrete, the shear stress on the crack surface is mainly due to aggregate interlock, and the empirical formula for the aggregate interlock now is suitable to model the shear behavior of the discrete cracks, which will be explained in later content. So if a linear softening branch of stress-strain relationship of cracked concrete is adopted (Peterson 1981, Bazant 2002), then

$$\varepsilon_{i,u} = \frac{2G_f}{f_t b} \quad (14)$$

where  $f_t$  is the tensile strength of concrete.  $b$  is the crack band width and it equals to the diameter of the influence domain of corresponding Gauss point.  $G_f$  is the fracture energy of concrete. It is proposed by CEB-FIP (1993) that:

$$G_f = \alpha \left( \frac{f_c}{10} \right)^{0.7} \quad (15)$$

where  $\alpha = 0.03$  for normal concrete and  $f_c$  (MPa) is the compressive strength of concrete.

In EFGM, the function of influence domain is just like the elements in finite element method, which is used to buildup the local approximate displacement field. And the polynomial  $\mathbf{p}(x)$ , which makes up the local approximate displacement field, is linear in this study (Eq. 2). So the crack band width  $b$  in EFGM is similar to the one in finite element methods with linear elements, which basically equals to the size of the elements, or the diameter of influence domain.

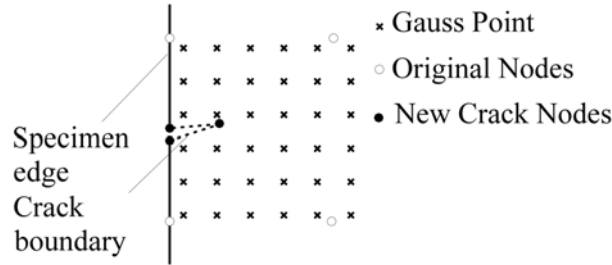


Fig. 2 Initiation of macro-crack

#### 4.2 Initiations of macro-cracks

Because the meshless method does not have any restraint from the element mesh, the cracks can be generated conveniently by adding nodes and boundaries in any place needed. Since the RC specimens studied in this paper are under bending or bending-shear combined load, it is assumed that all the macro-cracks initiates from the edge of the specimen in this computation. With this assumption, the complicated boundary intersection among crack boundaries and specimen edges can be avoided. More researches will be carried out in future study to simulate the intersection and separation of discrete cracks.

The detailed implementations for the initiates of macro-cracks are illustrated as follows:

- (1) In a certain load step, the tensile strain of point  $p_{ext}$  on the specimen edge is calculated by extrapolating the tensile strain of Gauss points near to the edge.
- (2) If the maximum extrapolated tensile strain on point  $p_{ext}$  is larger than  $\varepsilon_{t,u}$ , then there will be a macro-crack initiating from this point.
- (3) Two new nodes on both sides of  $p_{ext}$  will be added along the direction of specimen edge with a very small space  $\Delta_{c,i}$ . And another node  $N_c^t$  is added inside the specimen, which is located in the direction of principal compressive stress of  $p_{ext}$ , and this node is set to be crack tip node. The initial distance from  $N_c^t$  to  $p_{ext}$  is two times of the Gauss point space  $\delta_{gauss}$ . New boundaries are built with these three nodes, which are referred as crack boundaries, as shown in Fig. 2.
- (4) The relationship between node and Gauss point is rebuilt with new node distribution and new boundaries by the method introduced in Chapter 3. The current load step is calculated again to obtain the maximum tensile strain  $\varepsilon_{c,t}^t$  on the crack tip node  $N_c^t$ .
- (5) If  $\varepsilon_{c,t}^t > \varepsilon_{t,u}$ , which means the length of the new crack should be larger than current one, the crack length will be increased by extending  $N_c^t$  to one more  $\delta_{gauss}$  along the current crack direction.
- (6) Step (4) and (5) are iterated until  $\varepsilon_{c,t}^t < \varepsilon_{t,u}$ . Then it is regarded that the propagation of this macro-crack is finished in the current load step.

It should be mentioned that there might be strain concentrations problem on the crack tip. And if the node spacing or the crack propagation segment is too large, it will cause serious convergence problem, and the shape of crack will be influenced by the initial node distributions. Munjiza *et al.* (1999) have given a detailed discussion on this problem and they found that the maximal initial node space  $h$  should be much smaller than the length of micro-crack zone  $\Delta_{cr}$  to avoid such problems. As the micro-crack zone changes during the computation, Munjiza *et al.* (1999) proposed

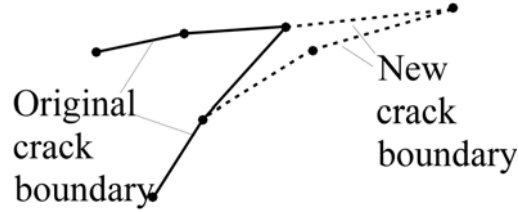


Fig. 3 Propagation of macro-crack

the following equations to roughly estimate the size of  $\Delta_{cr}$ :

$$\Delta_{cr} = \frac{\pi E \delta_c}{32 f_t} \sim \frac{E \delta_c}{4 f_t} \tag{16}$$

where  $E$  is the elastic modulus of concrete,  $\delta_c$  is the width of crack when the residual tensile stress of cracked concrete decreases to zero.  $f_t$  is the tensile strength of concrete. So, for a normal concrete with a tensile strength  $f_t = 3$  MPa, compressive strength  $f_c = 30$  MPa and elastic modulus  $E = 30$  GPa, with Eq. (15) the fracture energy of concrete  $G_f = 0.0647$  MPa mm, and the softening branch of cracked concrete is set to be a linear curve, then

$$\delta_c = 2 G_f / f_t = 4.32 \times 10^{-2} \text{ mm} \tag{17}$$

So with Eq. (16), the length of micro-crack zone  $\Delta_{cr} = 42.4 \sim 108$  mm.

Hence, in this study, the average space of initial node distribution  $h$  is set to be about 10 mm to give a stable numerical result.

### 4.3 Propagation of macro-cracks

When a new load step is applied, the tensile strain at every crack tip node  $N_{c,i}^t$  is calculated. If the maximum tensile strain of  $N_{c,i}^t$  is larger than  $\varepsilon_{i,u}$ , a new node  $N_1$  is added which is very close to  $N_{c,i}^t$ , and another new node  $N_2$  is added which is advanced for about  $2 \delta_{gauss}$  in the direction of maximum compression strain of  $N_{c,i}^t$ . The relationship of new nodes is shown in Fig. 3.

Set  $N_2$  to be new crack tip, modify the relationship of nodes and Gauss points, and recalculate current load step. If the maximal tensile strain on the new crack tip node  $N_2$  is larger than  $\varepsilon_{i,u}$ , then  $N_2$  is further moved along the original direction for  $\delta_{gauss}$  space. This process is iterated until the maximal tensile strain on the new crack tip node  $N_2$  is smaller than  $\varepsilon_{i,u}$ .

### 4.4 Crack surface elements

From the macro-cracks obtained by the above process, it is very convenient to stimulate the opening and sliding of crack surface. Hence, the shear stress-slip relationship for the aggregate interlock in the crack surface can be used directly, just like their successful application in discrete crack models (Elfgrén 1989). It should be mentioned that shear behavior of cracked concrete is a very complicated phenomenon. Currently better understanding has been achieved for well-developed cracks in which shear stress is mainly due to aggregate interlock, but little has been obtained for the shear mechanism of micro-cracks, in which shear stress is a combined effect of aggregated

interlock, crack surface friction and residential shear strength of concrete. In smeared crack model, an empirical shear modulus  $G_c$  for cracked concrete is usually used instead of elastic shear modulus  $G_0$  to represent the shear stiffness reduction due to cracking (Rots *et al.* 1985, Rots and Blaauwendraad 1989, Lu *et al.* 2005). And it is found that this empirical shear modulus gives a good representation for cracks with smaller opening and shear sliding but a poor result for well-developed cracks (Rots *et al.* 1985, Rots and Blaauwendraad 1989), because the opening and sliding of well-developed cracks cannot be precisely described with the even-distributed cracking strains in smeared crack model. At the same time, most crack surface shear tests are based on well-developed cracks because it is very difficult to control the crack width in micro-cracks. Hence, in this study, it is rational that the empirical shear modulus  $G_c$  is still used for smeared crack model that represent the micro-cracks, in which  $G_c$  not only represents the aggregated interlock but also represents the residential cohesive shear stress in concrete when crack is very small. And when cracks become macro-ones, and the shear force in the crack face is mainly due to aggregated interlock, an empirical relationship of shear stress vs. slip in the crack surface is adopted which is based on the research of Fenwick and Pauley (1968):

$$\tau_a = (3.218/w - 2.281)(0.271 \sqrt{f_c} - 0.409)(\Delta - 0.0436w) \quad (18)$$

where  $\tau_a$  is the shear stress in the crack surface caused by aggregate interlock (MPa).  $w$  is the crack width (mm).  $f_c$  is the uniaxial compressive strength of concrete (MPa).  $\Delta$  is the relative sliding displacement of crack surface (mm).

Once there is a macro-crack occurs or propagates, a spring element, which is referred as crack surface element here, is added together with the new node pair of the macro-crack. The direction of the spring is parallel to the crack surface, so as to bear the shear force. The tangent stiffness of the spring is shown as follows:

$$K = \frac{\partial \tau_a}{\partial \Delta} l t = (3.218/w - 2.281)(0.271 \sqrt{f_c} - 0.409) l t \quad (19)$$

where  $l$  is the incremental length of the macro-crack and  $t$  is the thickness of concrete.

## 5. Different smeared crack models

There are two types of smeared crack models used most widely in the finite element analysis of concrete. One is referred as Fixed-crack-model (FCM). The other is referred as Rotating-crack-model (RCM) (Rots and Blaauwendraad 1989, Weihe *et al.* 1998). The main difference between the two models is: After the first crack initiates in a certain Gauss point, FCM assumes that the direction of crack will not change anymore, while RCM assumes the crack direction will always perpendicular to the maximum tensile stress.

From theoretical analysis, when cracks firstly initiate, they are very small and they do not show strong directional consistency due to the random distribution of aggregates and initial voids. And the major crack directions are able to change with further stress development. However, with the increase of damage, when the cracks are wide enough, the micro-cracks connected with each other to become a macro-one, so the major crack directions cannot rotate freely parallel with the principal stress. Hence, because FCM assumes the crack angle will not change once the crack appears, it will

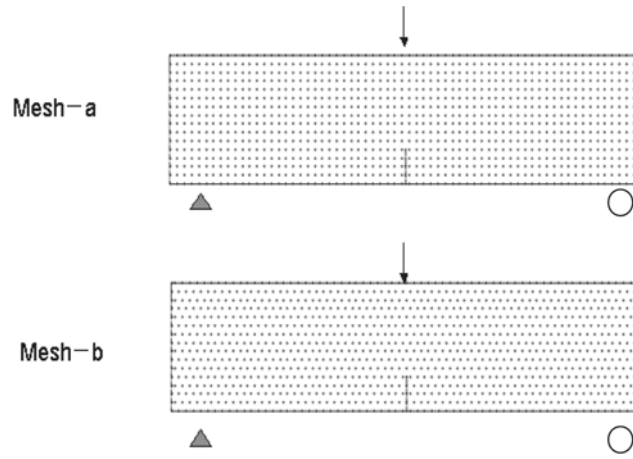


Fig. 4 3-point bending beams



(a) Mesh-a, FCM+ Discrete crack



(b) Mesh-b, FCM+ Discrete crack (Converge tolerance =2% )



(c) Mesh-b, FCM+ Discrete crack (Converge tolerance =1% )



(d) Mesh-a, RCM+ Discrete crack (Converge tolerance =2% )



(e) Mesh-b, RCM+ Discrete crack

Fig. 5 Crack patterns with FCM or RCM

overestimate the initial damage of early cracking. On the contrary, RCM assumed crack direction is always consistent with principal stress, so it may underestimate the influence of opened cracks. Then it is reasonable to use RCM firstly when the cracks are relatively small, and to fix the direction of crack when the cracks are wide enough. Consequently, in the composite crack model in this study, RCM should be more feasible for the micro-crack stage.

In order to verify the conclusion above, numerical tests are carried out to compare RCM and FCM in current composite crack model. A plain concrete 3-point bending beam with a notch in the mid span is analyzed, with two types of node distribution as shown in Fig. 4. The macro-crack pattern with the composite crack model discussed above is shown in Fig. 5. It should be mentioned that during the crack propagation in Mesh B, it will closely pass several existing nodes. Then the macro-cracking path has to leave the symmetric section of the beam to avoid the separations of existing nodes. At this time, crack propagation will be affected by the accumulated errors of numerical iterations. Because the boundary constraint of right sliding support of the beam is weaker than the left hinge support, the accumulated error always leads the asymmetric cracking to go to the right side of the mid-section. Then, with FCM, the crack will keep on going to the right side of the beam because the initial error of crack direction cannot be eliminated in later iteration. If stricter convergence tolerance is given, which is reduced from Fig. 5(b) with a 2% residential force to Fig. 5(c) with a 1% residential force, the rotation of macro-cracks with FCM will be reduced but more efforts are needed to get a converged result. On the contrary, because the crack direction of RCM is able to change with the principal stress, the initial error of crack direction will be reduced in later iteration so that RCM can effectively reduce the influence of mesh bias and the cracking is always close to symmetric (Figs. 5d, e). So it can be concluded that RCM is preferred over FCM in micro-crack stage.

## 6. Combination of concrete and rebar

Since node distribution in the meshless method is very flexible, nodes can be placed in any place where rebar is located. Truss element which is often used to model discrete rebar is adopted in this analysis. The rebar and concrete share the same node to achieve a compatible displacement, which is shown in Fig. 6. The contribution of rebar stiffness is added to the global concrete matrix of EFGM.

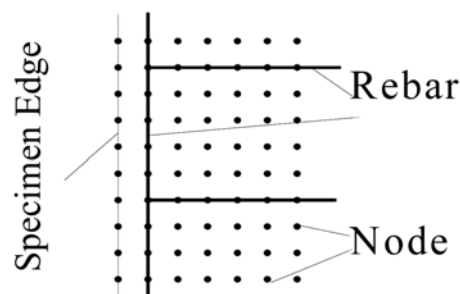


Fig. 6 Connection between rebar and concrete

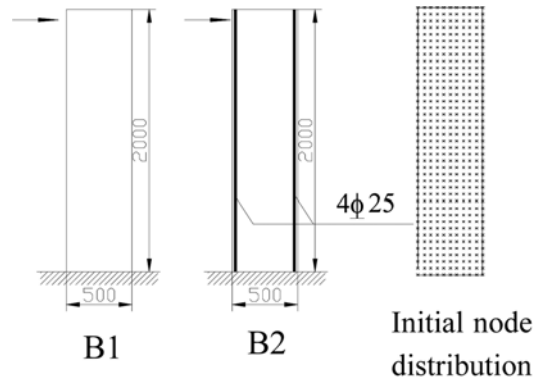


Fig. 7 Dimension and initial node distribution of specimens

## 7. Examples

### 7.1 Flexural failure of concrete beams

A plain concrete cantilever beam and a flexural reinforced concrete cantilever beam without stirrups are analyzed with the proposed model. The dimension and initial node distribution are shown in Fig. 7. Altogether  $41 \times 11 = 451$  nodes and 1600 Gauss points are used. The size of beams is  $2000 \times 250 \times 500$  mm. The cover layer thickness of B2 is 25 mm. The cube compression strength of concrete is 30 MPa, and the equivalent compression stress-strain curve advised in “Chinese code for design of concrete structure” (GB 2002) is adopted for concrete in this analysis, which is shown as follows.

$$\begin{cases} y = a_a x + (3 - 2a_a)x^2 + (a_a - 2)x^3 & x \leq 1 \\ y = \frac{x}{a_d(x - 1)^2 + x} & x > 1 \end{cases} \quad (20a)$$

$$\begin{cases} y = \frac{x}{a_d(x - 1)^2 + x} & x > 1 \end{cases} \quad (20b)$$

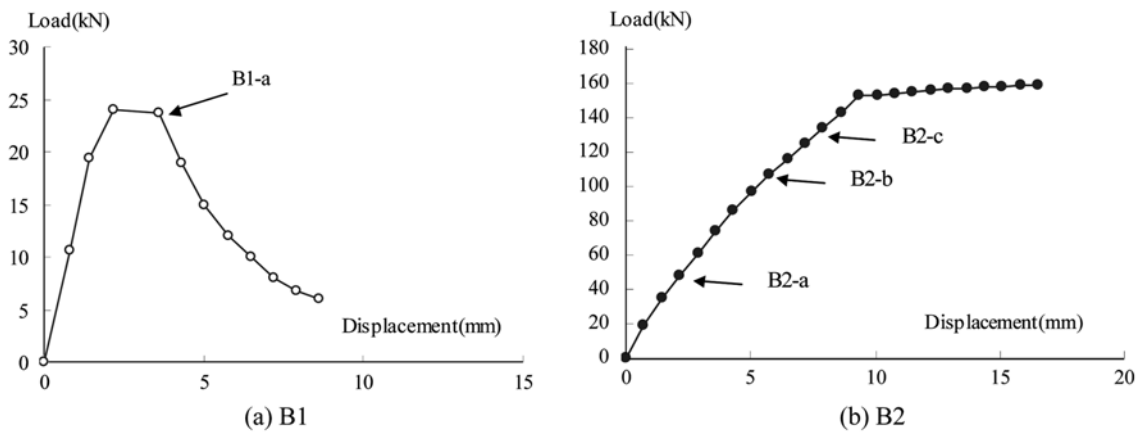


Fig. 8 Load-displacement curves for B1 & B2

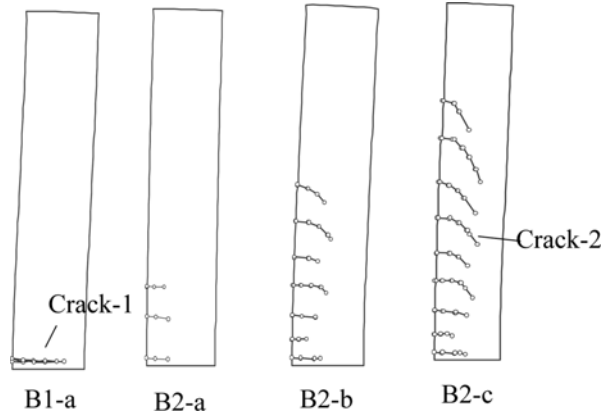


Fig. 9 Propagation of macro-cracks

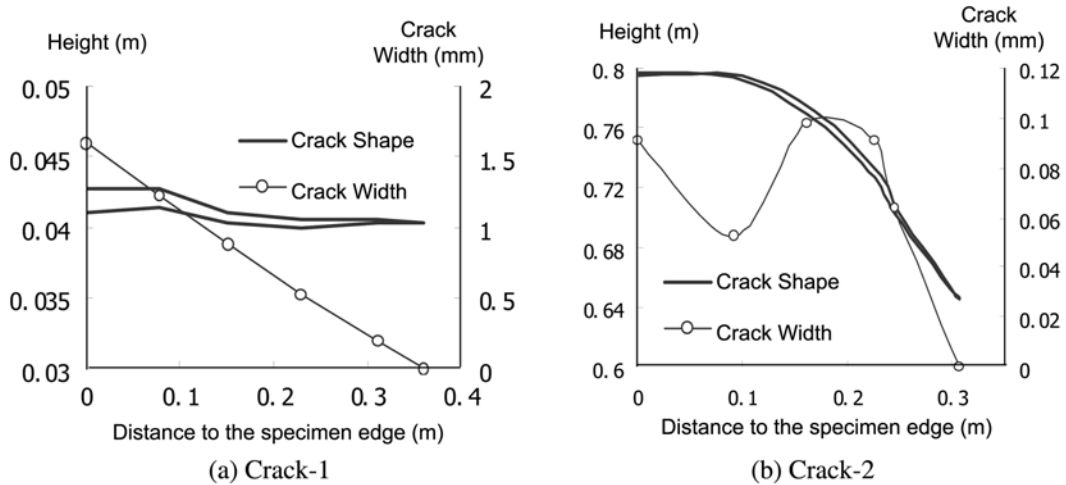


Fig. 10 Shape and width of selected cracks

where  $x = \varepsilon/\varepsilon_c$ ,  $y = \sigma/f_c$ .  $f_c$  is the uniaxial compression strength. And  $\varepsilon_c$  is the compress strain when  $\sigma = f_c$ .  $a_a$  and  $a_d$  are factors. According to the Chinese code (GB 2002),  $a_a = 2.03$ ,  $a_d = 1.36$ ,  $\varepsilon_c = 1640 \mu\varepsilon$ . The softening branch of stress-strain curve of cracked concrete is linear and the strain corresponding to the end of softening branch is given in Eq. (14).

The rebar material has a yield strength of 335 MPa, with perfect elasto-plastic flow after yielding. The load-displacement curves of the beam are shown in Fig. 8. The errors of strength and stiffness of numerical results are less than 10%, which are compared with the empirical model of Chinese code (GB 2002). The development of macro-cracks is shown in Fig. 9. It can be seen that this method can correctly simulate the deformation and crack development of concrete beams.

Two typical cracks, Crack-1 and Crack-2, in Fig. 9, are selected and magnified in Fig. 10. In Crack-1, because there is no reinforcement in the beam, the width of this crack changes almost linearly for the edge of the specimen to the crack tip. However, for Crack-2, the crack width is relatively small around the rebar due to the rebar's constraint. And the largest crack width is found in the middle of the specimen because there is no stirrup in this beam. All these are very consistent with test results.

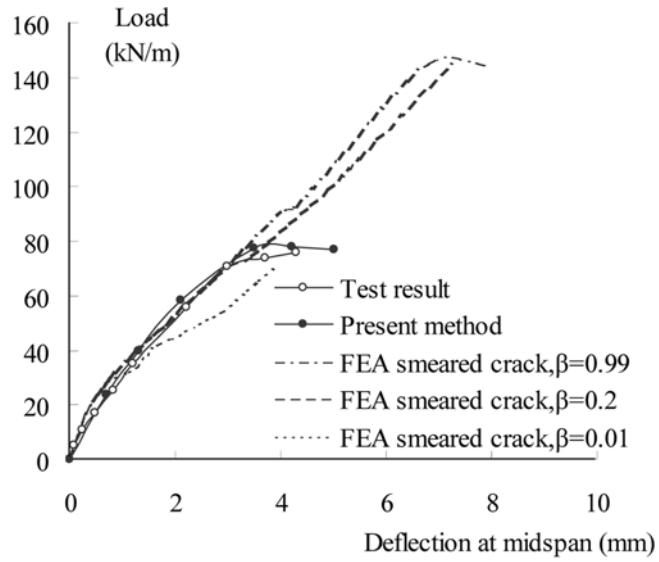
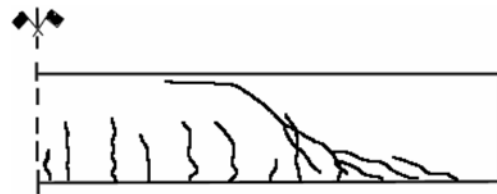
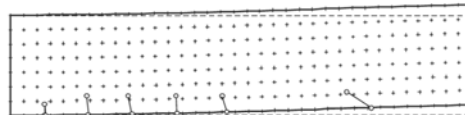


Fig. 11 Comparison of load-displacement curves



(a) Cracks in the test



(b) Numerical result  
(deflection at midspan=2.1mm)



(c) Numerical result  
(deflection at midspan=5.1mm)

Fig. 12 Development of cracks

## 7.2 RC beam fails in diagonal tension

A reinforced concrete beam without stirrups failing in diagonal tension was tested by Gijssbers and Smit (Rots *et al.* 1985), and analyzed by Rots *et al.* (1985) with smeared crack model based on finite element method. As in such type of beams, the aggregate interlock plays an important role for the shear capacity, a proper shear retention factor  $\beta$  is important to obtain a precise prediction. Although many shear retention models have been developed for smeared crack model (Zhu *et al.* 2001), it is still difficult for smeared crack model alone to deal with such problems. However, with the composite crack model discussed above, the aggregated interlock on the critical shear crack surface can be precisely modeled with the empirical equation based on crack shear test. The numerical results are shown in Figs. 11 and 12 (finite element smeared crack results were computed by Rots *et al.* 1985). In the early stage of the load, when the deflection at the mid-span is about 2.1 mm, because no shear reinforcement is inside the beam, the micro-cracks with smeared crack model cover about 2/3 of the beam height from the bottom. However, most micro-cracks are very small and only 5 flexural macro-cracks take place in the middle span of the beam due to flexure, whilst one more macro-crack initiates near the support due to the local stress concentration (Fig. 12b). With load increase, the development of macro-cracks are mainly the propagation of existing macro-cracks in early load stages. Only two more macro-cracks appear due to the large anchorage stress of the reinforcement when diagonal shear crack is well developed (Fig. 12c). Because in current composite crack model the macro-cracks cannot intersect with each other, the final complicated cracking of concrete near to the bottom of diagonal shear crack (Fig. 12a) cannot be fully simulated. After all, the proposed model correctly simulates the propagation of diagonal shear crack and gives a precise prediction of peak shear load and corresponding deflection (Fig. 11).

## 8. Conclusions

A novel composite crack model based on meshless method, which combines smeared and discrete crack models, is introduced in this paper. The cracks in concrete are classified and modeled with different cracking approaches. The detailed implementation for the initiation and propagation of macro-cracks is presented, with the advantages of meshless method. FCM and RCM are compared and RCM is proved to be able to reduce the mesh bias influence. The numerical examples show that this method can correctly simulate the shape and propagation of macro-cracks.

## Acknowledgements

This research is financial supported by the China National Natural Science Fund (project number: 50278047) and the Cultivation Fund of the Key Grant Scientific and Technical Innovation Project, Ministry of Education of China (No.704003).

## References

Areias, P.M.A. and Belytschko, T. (2005), "Analysis of three-dimensional crack initiation and propagation using

- the extended finite element method”, *Int. J. Numer. Meth. Eng.*, **63**(5), 760-788.
- Bazant, Z.P. (2002), “Concrete fracture models: Testing and practice”, *Eng. Fracture Mech.*, **69**, 165-205.
- Bazant, Z.P. and Planas, J. (1997), *Fracture and Size Effect in Concrete and other Quasibrittle Materials*. Boca Baton: CRC Press.
- Belytschko, T. (1996), “Meshless method: An overview and recent development”, *Comput. Meth. Appl. Mech. Eng.*, **139**, 3-47.
- Belytschko, T. and Lu, Y.Y. (1994), “Element free Galerkin method”, *Int. J. Numer. Meth. Eng.*, **37**, 229-256.
- CEB-FIP (1993), *Model Code 90*. Lausanne.
- Elfgren, L. (1989), *Fracture Mechanics of Concrete Structure, from theory to Applications*. London: St Edmundsbury Press.
- Fenwick, R.C. and Pauley, T. (1968), “Mechanisms of shear resistance of concrete beams”, *J. ACI*, **94**(10), 2325-2350.
- Gasser, T.C. and Holzapfel, G.A. (2005), “Modeling 3D crack propagation in unreinforced concrete using PUFEM”, *Comput. Method Appl. Mech. Eng.*, **194**(25-26), 2859-2896.
- GB (2002), *Code for Design of Concrete Structure GB 50010-2002*. Beijing: China Building Industry Press, 206-208.
- Grootenboer, H.J., Leijten, S.F.C.H. and Blaauwendraad, J. (1981), “Concrete mechanics, Part C, Numerical models for reinforced concrete structures in plane stress”, *HERON*, **26**(1c), 15-41.
- Jiang, J.J., Lu, X.Z. and Ye, L.P. (2005), *Finite Element Analysis of Concrete Structures*. Beijing: Tsinghua University Press.
- Jirasek, M. and Zimmerman, T. (1998), “Rotating crack model with transition to scalar damage”, *J. Eng. Mech.*, ASCE, **124**(3), 277-284.
- Liu, G.R. (2002), *Mesh Free Methods: Moving Beyond the Finite Element Method*, Boca Baton: CRC Press, 2002.
- Loblein, J. and Schroder, J. (2005), “Numerical simulation of crack problems using triangular finite elements with embedded interfaces”, *Comput. Mater. Sci.*, **32**(3-4), 435-445.
- Lu, X.Z., Ye, L.P., Teng, J.G. and Jiang, J.J. (2005), “Meso-scale finite element model for FRP sheets/plates bonded to concrete”, *Eng. Struct.*, **27**(4), 564-575.
- Luis Gavete, J.J. and Benito, S.F. (2000), “Penalty functions in constrained variational principles for element free Galerkin method”, *Eur. J. Mech. A/Solids* **19**, 699-720.
- Munjiza, A. (2004), *The Combined Finite-Discrete Element Method*. London: Wiley & Sons.
- Munjiza, A., Andrews, K.R.F. and White, J.K. (1999), “Combined single and smeared crack model in combined finite-discrete element method”, *Int. J. Numer. Meth. Eng.*, **44**, 41-57.
- Peterson, P.E. (1981), “Crack growth and development of fracture zone in plain concrete and similar material”, Doctoral dissertation, Lund Institute of Technology, Sweden, 174.
- Rots, J.G. and Blaauwendraad, J. (1989), “Crack models for concrete: discrete or smeared? Fixed, multi-directional or rotating?”, *HERON*, **34**(1).
- Rots, J.G., Nauta, P., Kusters, M.A. and Blaauwendraad, J. (1985), “Smeared crack approach and fracture localization in concrete”, *HERON*, **30**(1).
- Schroder, J. and Loblien, J. (2005), “A geometric nonlinear triangular finite element with an embedded discontinuity for the simulation of quasi-brittle fracture”, *Comput. Mech.*, **36**(2), 139-157.
- Weihe, S., Kroplin, B. and de Borst, R. (1998), “Classification of smeared crack models based on material and structural properties”, *Int. J. Solids Struct.*, **35**(12), 1289-1308.
- Wells, G.N. and Sluys, L.J. (2000), “Application of embedded discontinuities for softening solids”, *Eng. Fracture Mech.*, **65**, 263-281.
- Zhou, W.Y. and Kou, X.D. (1998), “Meshless method and engineering application”, *Aeta Mechancia Sinia*, **30**(2), 193-202.
- Zhu, R.H. Thomas, T.C. and Lee, J.Y. (2001), “Rational shear modulus for smeared-crack analysis of reinforced concrete”, *ACI Struct. J.*, **98**(4), 443-450.
- Zi, G. and Belytschko, T. (2003), “New crack-tip elements for XFEM and applications to cohesive cracks”, *Int. J. Numer. Meth. Eng.*, **57**(15), 2221-2240.

**Notation**

$\mathbf{a}(x)$	: factor vector for moving least square (MLS) computation
$B$	: shape function matrix
$E$	: elastic modulus of concrete
$f_c$	: uniaxial compression strength of concrete
$G_f$	: fracture energy for concrete
$h$	: maximal initial node space
$K$	: global stiffness matrix for EFG
$l$	: increment of the macro-crack length
$n(x)$	: shape function obtained from MLS
$n_i(x)$	: partial difference of shape function $n(x)$
$\mathbf{p}(x)$	: $m$ dimensional polynomial
$r_m$	: radius for influence domain in EFGM
$t$	: thickness of concrete specimen
$w(\ x - x_j\ )$	: weight function in moving least square (MLS) computation
$w$	: crack width (mm)
$\beta$	: shear retention factor
$\delta_c$	: the width of crack when the residual tensile stress of cracked concrete decreases to zero
$\delta_{gauss}$	: Gauss point space
$\Delta$	: relative sliding displacement of crack surface (mm)
$\Delta_{cr}$	: length of micro-crack zone
$\Delta_{c,i}$	: initial macro-crack width
$\varepsilon_{t,u}$	: critical value of tensile strain to transmit the smeared model to discrete model
$\varepsilon_{c,t}^t$	: tensile strain on the crack tip
$\tau_a$	: shear stress on the crack surface caused by aggregate interlock